Available online at www.sciencedirect.com
ScienceDirect
Journal of Power Sources 164 (2007) 730–741
JOURNAL OF POWER SOURCES
www.elsevier.com/locate/jpowsour

Numerical prediction of the effect of catalyst layer Nafion loading on the performance of PEM fuel cells

Chin-Hsiang Cheng [a,*], Hung-Hsiang Lin [b], Guang-Jer Lai [b]

[a] *Department of Aeronautics and Astronautics, National Cheng Kung University, No. 1, Ta Shieh Road, Tainan 70101, Taiwan, ROC*
[b] *Department of Mechanical Engineering, Tatung University, Taipei 10451, Taiwan, ROC*

Received 20 October 2006; received in revised form 19 November 2006; accepted 20 November 2006
Available online 3 January 2007

Abstract

Numerical simulations are performed to investigate the effect on PEM fuel cell performance of Nafion loading in the catalyst layer. The investigation also considers variations of geometric parameters. A model that accounts for the volume fractions of Nafion, the solid catalyst particles, and the void space inside the catalyst layers is incorporated into a three-dimensional computational fluid dynamics code, capable of resolving three-dimensional mass, momentum, and species transport phenomena as well as the electron- and proton-transfer processes in a PEMFC. Numerical results are first compared with experiments, showing close agreement between predictions and measurements. A parametric study on the effects of Nafion loading and geometric parameters variation is carried out to evaluate the performance of PEMFC for various parameter combinations.

Keywords: Nafion loading; PEMFC; Parametric study; Prediction; Experiment

1. Introduction

Fuel cells are an important technology for a potentially wide variety of applications including auxiliary power, transportation power, and stationary power for buildings and other distributed generation applications. These applications are encountered in a large number of industries worldwide.

In the electrochemical reactions of the proton exchange membrane fuel cells (PEMFC), hydrogen at the anode provides protons, freeing electrons in the process that must pass through an external circuit to reach the cathode. The protons, which remain solvated with a certain number of water molecules, migrate through the membrane to the cathode to react with oxygen and the returning electrons. Water is subsequently produced at the cathode. In a PEMFC, Nafion is used as the membrane placed between the anode and the cathode. Furthermore, it is also employed as an important component of the active layer in the catalyst layer. The content of Nafion in the catalyst layers affects simultaneously the gas permeability, the catalytic activity and the ionic resistance. Hence, an optimal Nafion content in the catalyst layer is definitely desired for good performance.

Introducing Nafion into the catalyst layer makes the layer active in three dimensions because the protons can then be transported throughout the entire layer. Boyer et al. [1] reported that the ionic conductivity of the catalyst layer increases with the volume fraction of Nafion in the composite mixture, and the authors derived several expressions for determining the optimum thickness, Pt loading and Nafion content for the electrodes by considering these variables as the single variable in these expressions. According to the reports given by Passalacqua et al. [2,3] and Antolini et al. [4], it is found that since Nafion is an electronic insulator, it decreases the electronic conductivity of the catalyst layer, and may cause some catalyst particles to be electronically isolated. These isolated particles will not be able to participate in any electrochemical reactions. In addition, Nafion will change the porosity, permeability, and hydrophobicity of the catalyst layer. Therefore, the Nafion content in the catalyst layer needs to be precisely controlled in order to achieve the best balance among all these influencing factors. Qi and Kaufman [5] simply mixed the carbon-supported catalysts with Nafion without adding any extra material. In this report, it was observed that the performance increased with Nafion content up to 30%, and it

* Corresponding author. Tel.: +886 6 2757575x63627; fax: +886 6 2389940.
E-mail address: chcheng@mail.ncku.edu.tw (C.-H. Cheng).

0378-7753/$ – see front matter © 2006 Elsevier B.V. All rights reserved.
doi:10.1016/j.jpowsour.2006.11.039

Nomenclature

a	water activity
D	mass diffusivity ($m^2\ s^{-1}$)
F	Faraday constant, 96487 C mol^{-1}
h	height of gas channel (m)
i	local electric current density ($A\ m^{-3}$)
$\bar{i}$	local ionic current density ($A\ m^{-3}$)
$\mathbf{I}$	electric current density ($A\ m^{-2}$)
j	transfer current density ($A\ m^{-3}$)
k	permeability (m^2)
l_C	gas channel width (m)
l_L	gas channel length (m)
l_P	width of a module (m)
M	molecular weight (kg $kmol^{-1}$)
n	coordinate in the direction normal to the surface
P	pressure (Pa)
$\mathbf{P}$	power density ($W\ m^{-2}$)
r	concentration parameter
R	universal gas constant, 8.314 J $mol^{-1}\ K^{-1}$
S	source term in species equation
t_{Cat}	thickness of catalyst layer (m)
t_{GDL}	thickness of gas diffusion layer (m)
t_m	thickness of membrane (m)
t_P	thickness of carbon plate (m)
T	temperature (K)
$\vec{U}$	gas velocity vector ($m\ s^{-1}$)
v_N	volume occupied by Nafion in catalyst layer
v_S	volume occupied by solid catalyst particles in catalyst layer
v_t	total volume of catalyst layer
v_V	volume of void space in catalyst layer
V	inlet gas velocity ($m\ s^{-1}$)
$\mathbf{V}$	cell voltage (V)
X	mole fraction
x, y, z	Cartesian coordinates
Y	mass fraction

Greek letters

α	transfer coefficient for the reaction
χ	Bruggemann coefficient
ε_{GDL}	porosity of gas diffusion layer
$\varepsilon_{N,Cat}$	volume fraction of Nafion in catalyst layer
$\varepsilon_{S,Cat}$	volume fraction of solid catalyst particles in catalyst layer
$\varepsilon_{V,Cat}$	volume fraction of void space (porosity) in catalyst layer
ϕ	electric potential (V)
φ	phase potential (V)
Γ_m	ionic conductivity of membrane ($\Omega^{-1}\ m^{-1}$)
$\Gamma_{N,Cat}$	ionic conductivity of Nafion ($\Omega^{-1}\ m^{-1}$)
λ	membrane water content, kmol H_2O (kmol SO_3^-)$^{-1}$
Λ	gas channel width fraction
ρ	density of oxygen ($kg\ m^{-3}$)
σ_{GDL}	electronic conductivity of gas diffusion layer ($\Omega^{-1}\ m^{-1}$)
σ_P	electronic conductivity of carbon plate ($\Omega^{-1}\ m^{-1}$)
$\sigma_{S,Cat}$	electronic conductivity of solid catalyst particle ($\Omega^{-1}\ m^{-1}$)
τ	fluid stress ($N\ m^{-2}$)
ζ	source term in electronic conduction equation

Subscripts

a	anode
c	cathode/gas channel
Cat	catalyst layer
eff	effective
GDL	gas diffusion layer
i	inlet
m	membrane
N	Nafion
o	outlet
P	carbon plate
ref	reference
S	solid catalyst particles

decreased afterwards. Their experimental data showed that the best performance was achieved with Pt loading of 0.2 ± 0.05 and 0.35 ± 0.05 mg cm^{-2}, for 20 and 40% Pt/C support, respectively. In addition, Lufrano et al. [6] investigated the effects of Nafion loading in electrodes on the performance of supercapacitors by electrochemical impedance spectroscopy. The capacitors, with lower Nafion content but having higher conductivities and better capacitance performances, were obtained.

Numerical methods have been employed to study the physical phenomenon of interest in the fuel cells since these methods require relatively lower cost for analysis than the experimental ones. Furthermore, they in general provide a sufficient amount of data not easily obtainable with measurements. Thus, important natures of the flow and the thermal fields might then be observed and discussed extensively by numerical studies. To name a few, Wang and Savinell [7] performed a simulation of the effects of porosity and thickness of the catalyst layer, Pt loading, and CO poisoning on fuel cells. Yi and Nguyen [8] used the numerical methods to solve a two-dimensional single-phase PEMFC model with interdigitated flow channels so as to evaluate the effects of inlet and exit pressures, gas diffusion layer thickness, and carbon plate width on the performance of PEMFC. Gurau et al. [9] developed a half-cell model to deal with the transport phenomena at the cathode of the PEMFC. The research explored the effects of the porosity of the gas diffusion layer on the performance of fuel cells. More recently, Lin et al. [10] investigated the optimization of the proton exchange membrane fuel cell. A simplified conjugate-gradient method (SCGM) is employed to seek the optimal combination of the design parameters, including the channel width ratio, the porosity of GDL, and the porosity of the catalyst layer.

As to the three-dimensional models, Hontanon et al. [11] adopted a commercial computational fluid dynamics code (FLUENT) to predict the effects of a group of geometrical parameters on the polarization performance of the fuel cells. Berning and Djilali [12] used a three-dimensional physical model to evaluate the performance of the fuel cells at different operating conditions. Their research showed that an increase in the fuel cell temperature could raise the cell exchange current density, ionic conductivity of proton exchange membrane, gas diffusivity, and the operating voltage and then lead to an increase in the cell performance.

In spite of the valuable experiments performed by many groups [1–6] to investigate optimal Nafion content in the catalyst layers, theoretical information on the effects of Nafion loading is relatively scarce. Reliable information about the fuel cell behavior may be collected by experimental or numerical methods. However, unfortunately, so far only a limited number of theoretical reports have been presented. Among the very few theoretical works, Song et al. [13] proposed an optimization problem for the cathode catalyst layer performance by assuming that the Nafion content and Pt loading are uniformly distributed in the cathode catalyst layer. From this, the optimal Nafion content, Pt loading, and layer thickness were determined. In a recent report [14], the same group of authors studied the optimal distributions of Nafion content and Pt loading across the entire thickness of cathode catalyst layers, which was obtained by maximizing the cell current density at a given potential. When optimization was performed with either the Nafion content or Pt loading as the single variable, authors found that the optimal distribution is a linearly increasing function from the gas diffusion layer side to the membrane side. Secanell et al. [15] addressed the same topic using a two-dimensional model and solved for the catalyst layer composition using a multivariable optimization technique.

With the help of theoretical study, the basics of the improvement of fuel cell performance by Nafion loading might be clarified and the optimal Nafion content could be determined. In these circumstances, the present study is aimed to investigate the influence of Nafion loading in the catalyst layers on the behavior of a proton exchange membrane fuel cell by numerical simulation. In this study, a self-developed subroutine, which is used to deal with the volume fractions of Nafion loaded, solid catalyst particles, and void space inside the catalyst layers, is incorporated with a three-dimensional computational fluid dynamics code, which is capable of dealing with the three-dimensional mass, momentum, and species transport phenomena as well as the electron- and proton-transfer process taking place in the PEMFC.

Numerical predictions of the Nafion loading effects by using a full-cell three-dimensional model are presented. In addition, a 22 cm × 22 cm single-cell fuel cell module with 14 cm × 14 cm active area has been installed and tested. Numerical results are compared with the experiments for validation. A comprehensive parametric study of the effects of the parameters including volume fraction of Nafion in the catalyst layer, volume fraction of void space in the catalyst layer, gas channel width fraction, thickness and porosity of gas diffusion layer, and membrane thickness has been further carried out to evaluate the performance of PEMFC under various combinations of these parameters.

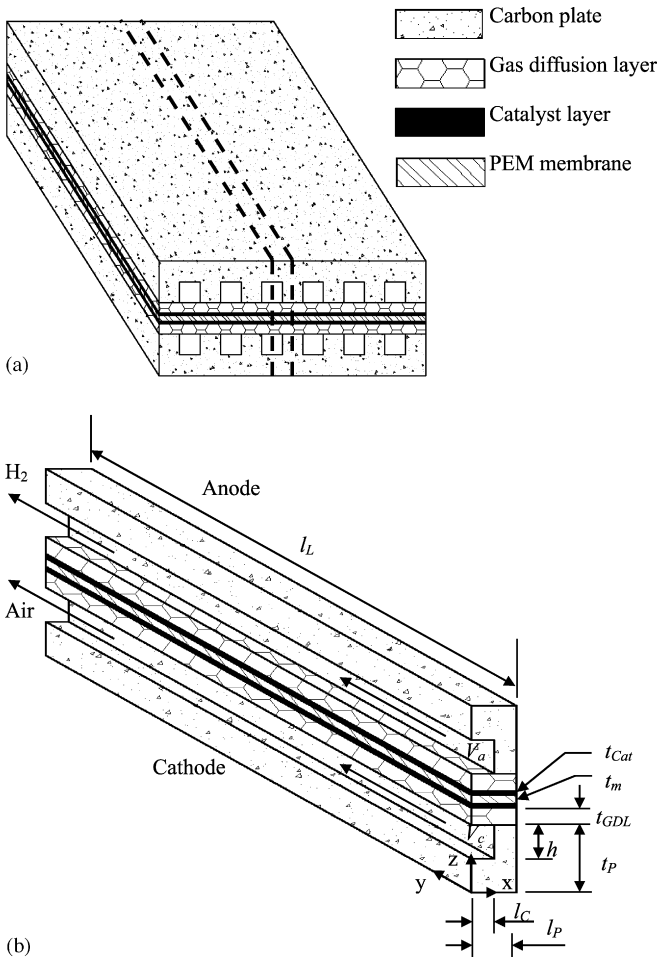

Fig. 1. Schematic of a single-cell proton exchange membrane fuel cell. (a) Single cell with parallel straight channels and (b) flow channel geometry.

Schematic of a single-cell PEMFC with parallel straight channels on both the anode and the cathode carbon plates is shown in Fig. 1. The single-cell PEMFC consists of a carbon plate, a gas diffusion layer (GDL), a catalyst layer, for each of the anode and the cathode, as well as a PEM membrane at the center. Here the physical and geometrical parameters of the cell shown in this figure may be divided into two groups: the fixed and the varied parameters. For these fixed parameters, their values are kept constant throughout the study. On the other hand, as mentioned earlier, the volume fraction of Nafion in the catalyst layer ($\varepsilon_{N,Cat}$), the volume fraction of void space in the catalyst layer ($\varepsilon_{V,Cat}$), the gas channel width (l_C), the thickness and porosity of the gas diffusion layer (t_{GDL} and ε_{GDL}), and the membrane thickness (t_m) are regarded as major factors and are varied in this study in order to evaluate their effects. These parameters are referred to as the varied parameters. Values of the fixed parameters are listed in Table 1, and the variation ranges of these varied parameters are given in Table 2. Also provided in Table 2 are the values of the varied parameters for the base case, which is defined to be the test problem for the parametric study. Note that in this study, the operating temperature and pressure

Table 1
Fixed parameters in numerical simulation

Parameter	Symbol	Value
Operating temperature (K)	T	323
Inlet and outlet pressure (Pa)	P_i, P_o	101,325
Gas channel length (m)	l_L	5.0×10^{-2}
Width of a module (m)	l_P	1.0×10^{-3}
Thickness of catalyst layer (m)	t_{Cat}	1.0×10^{-5}
Thickness of carbon plate (m)	t_P	2.0×10^{-3}
Height of gas channel (m)	h	1.0×10^{-3}
Bruggemann coefficient of gas diffusion layer	χ_{GDL}	1.5
Bruggemann coefficient of catalyst layer	χ_{Cat}	1.5
GDL permeability (m^2)	k_{GDL}	1.76×10^{-11}
Catalyst layer permeability (m^2)	k_{Cat}	1.76×10^{-11}
Anode inlet gas velocity ($m\,s^{-1}$)	V_a	0.3
Cathode inlet gas velocity ($m\,s^{-1}$)	V_c	0.5
Anode inlet mass fraction of H_2	$Y_{H_2,i}$	0.445
Anode inlet mass fraction of H_2O	$Y_{H_2O,i}$	0.555
Cathode inlet mass fraction of O_2	$Y_{O_2,i}$	0.212
Cathode inlet mass fraction of N_2	$Y_{N_2,i}$	0.709
Cathode inlet mass fraction of H_2O	$Y_{H_2O,i}$	0.079
Operating voltage (V)	**V**	0.7
Anodic charge transfer coefficients for anode reaction	$\alpha_{a,a}$	0.5
Cathodic charge transfer coefficients for anode reaction	$\alpha_{a,c}$	0.5
Anodic charge transfer coefficients for cathode reaction	$\alpha_{c,a}$	1.5
Cathodic charge transfer coefficients for cathode reaction	$\alpha_{c,c}$	1.5
Reference transfer current density at anode ($A\,m^{-3}$)	$j_{a,ref}$	9.0×10^8
Reference transfer current density at cathode ($A\,m^{-3}$)	$j_{c,ref}$	250
Anode concentration parameter	r_a	1.0
Cathode concentration parameter	r_c	1.0
Electronic conductivity of gas diffusion layer ($\Omega^{-1}\,m^{-1}$)	σ_{GDL}	300
Electronic conductivity of carbon plate ($\Omega^{-1}\,m^{-1}$)	σ_P	4000
Electronic conductivity of catalyst layer ($\Omega^{-1}\,m^{-1}$)	$\sigma_{S,Cat}$	300
Ionic conductivity of Nafion ($\Omega^{-1}\,m^{-1}$)	$\Gamma_{N,Cat}$	25.56

Table 2
Varied parameters in numerical simulation

Parameter	Symbol	Base case	Variation range
Volume fraction of Nafion in catalyst layer	$\varepsilon_{N,Cat}$	0.3	0.1–0.8
Volume fraction of void space in catalyst layer	$\varepsilon_{V,Cat}$	0.112	0.05–0.65
Volume fraction of solid catalyst particles in catalyst layer	$\varepsilon_{S,Cat}$	0.588	0.05–0.788
Gas channel width (m)	l_C	5.0×10^{-4}	1.0×10^{-4} to 9.0×10^{-4}
Thickness of gas diffusion layer (m)	t_{GDL}	3.0×10^{-4}	0.5×10^{-4} to 5.0×10^{-4}
Porosity of gas diffusion layer	ε_{GDL}	0.5	0.1–0.9
Thickness of membrane (m)	t_m	1.78×10^{-4}	0.5×10^{-4} to 5.0×10^{-4}

are assigned to be 323 K and 101,325 Pa, respectively. The typical value of the operating voltage of the fuel cell is 0.7 V in the computation.

2. Theoretical analysis and numerical methods

The following assumptions are made in prior to the derivation of the governing equations:

1. the fuel cell operates at steady state;
2. the gas flows in the gas channels and the porous layers are laminar and compressible, and effects of buoyancy on the flow motion are negligible;
3. thermodynamic and electrochemical properties of the gases and the solid materials of the fuel cell components are assumed constant;
4. the operating temperature is uniform and constant in the solution domain;
5. the gas diffusion layers and the catalyst layers are homogeneous, isotropic porous media;
6. owing to high ohmic resistance of the membrane, the interface between the catalyst layer and the membrane is assumed to be insulated against electrons;
7. water exists in the entire fuel cell only in vapor phase, and no phase change process is taken into consideration.

2.1. Theoretical model

The present three-dimensional model involves (1) mass, momentum, and species transport phenomena in the gas channels and the porous layers, including the gas diffusion and the catalyst layers, (2) electrochemical reactions in the catalyst layers, (3) electronic conduction in the porous layers and the carbon plates, and (4) ionic conduction taking place in the catalyst layers and the proton exchange membrane. In addition, the theoretical model is applied to evaluating the influence of Nafion loading at various combinations of the volume fractions of Nafion loaded, solid catalyst particles, and void space in the catalyst layers. The governing equations of the theoretical model are described briefly in the following.

2.1.1. Mass, momentum, and species transport (gas channels, GDLs, and catalyst layers)

The governing equations for the gas flows in the gas channels and the porous layers are the conservation equations of mass, momentum, and species. Application of the flow channels and the gas diffusion layers in the fuel cells is to allow the reactant gases to diffuse uniformly into the catalyst layers but prevent excessive increase in electrical resistance against the released electrons from the catalyst layers. The porous layers include the gas diffusion layers and the catalyst layers, in which the mass, momentum, and species equations for the flows are derived based on the non-Darcy law. These equations are given below:

Mass equation:

$$\nabla \cdot (\varepsilon \rho \vec{U}) = 0 \tag{1}$$

Momentum equation:

$$\nabla \cdot (\varepsilon \rho \vec{U}\vec{U}) = -\varepsilon \nabla P + \nabla \cdot (\varepsilon \tau) + \frac{(\varepsilon)^2 \mu \vec{U}}{k} \tag{2}$$

Species equation:

$$\nabla \cdot (\varepsilon \rho U Y_i) = \nabla \cdot (D_i^{\text{eff}} \nabla Y_i) + S_i \tag{3}$$

where ε and k are the porosity and the permeability of the porous layers, respectively; τ represents the fluid stress tensor. Fuel gas at the anode is considered to contain H_2 and H_2O, and oxidant gas at the cathode contains O_2, N_2, and H_2O. Y_i denotes the species mass fraction of species i. Note that for the pure fluid flows in the gas channels, the values of ε and k are given with $\varepsilon = 1$ and $k = \infty$.

Calculation for the effective mass diffusivity of species i (D_i^{eff}) is based on Bruggemann's equation, that is

$$D_i^{\text{eff}} = (\varepsilon)^{\chi} D_i \tag{4}$$

where D_i is the mass diffusivity of species i and χ is the Bruggemann coefficient of the porous layer.

2.1.2. Electrochemical reaction (catalyst layers)

In Eq. (3), the term S_i stands for the source term of species i coming from the electrochemical reactions in the catalyst layers. Note that H_2 and O_2 are consumed by the reactions in the catalyst layers of anode and cathode, respectively, and H_2O is the product of the reaction at the cathode. Therefore, the source terms for different species are

$$S_{H_2} = -\frac{j_{\text{a}}}{2F} \tag{5a}$$

$$S_{O_2} = \frac{j_{\text{c}}}{4F} \tag{5b}$$

$$S_{H_2O} = -\frac{j_{\text{c}}}{2F} \tag{5c}$$

where j_{a} and j_{c} are the transfer current densities at the anode and the cathode, respectively, which are calculated based on the Butler–Volmer condition as

$$j_{\text{a}} = j_{\text{a,ref}} \left(\frac{Y_{H_2}}{Y_{H_2,\text{ref}}} \right)^{r_{\text{a}}} \times \left[\exp\left\{ \frac{\alpha_{\text{a,a}} F}{RT} \eta \right\} - \exp\left\{ \frac{-\alpha_{\text{a,c}} F}{RT} \eta \right\} \right] \tag{6a}$$

$$j_{\text{c}} = j_{\text{c,ref}} \left(\frac{Y_{O_2}}{Y_{O_2,\text{ref}}} \right)^{r_{\text{c}}} \times \left[\exp\left\{ \frac{\alpha_{\text{c,a}} F}{RT} \eta \right\} - \exp\left\{ \frac{-\alpha_{\text{c,c}} F}{RT} \eta \right\} \right] \tag{6b}$$

where $j_{\text{a,ref}}$ and $j_{\text{c,ref}}$ are the reference transfer current densities, and r_{a} and r_{c} the concentration parameters, at the anode and the cathode, respectively. In addition, $\alpha_{\text{a,a}}$ and $\alpha_{\text{a,c}}$ are the anodic and the cathodic charge transfer coefficients for anode reaction, and $\alpha_{\text{c,a}}$, and $\alpha_{\text{c,c}}$ the anodic and the cathodic charge transfer coefficients for cathode reaction. $Y_{O_2,\text{ref}}$ and $Y_{H_2,\text{ref}}$ are the reference concentrations at which the exchange current densities were obtained. All the reference values of these coefficients are already given in Table 1. Note that the reference current densities, transfer coefficients, and reference concentrations have been set so as to fit the experimental data.

2.1.3. Electronic conduction (carbon plates, GDLs, and catalyst layers)

The carbon plate, the GDL, and the catalyst layers all serve as conductors for electric current. In the carbon plate and the GDL, there is no electrochemical reaction taking place. The electrochemical reactions only take place in the catalyst layers. Due to the electrochemical reactions activated in the catalyst layers, there exists a source term in the electronic conduction equation. Therefore, in these three components the electronic conduction equation may be expressed in general form as

$$\nabla \cdot (\sigma^{\text{eff}} \nabla \phi) = \zeta \tag{7}$$

where ϕ is the electronic potential and σ^{eff} denotes the effective electronic conductivity. For the carbon plates, the effective electronic conductivity σ^{eff} is treated as a constant (σ_{P}). For the porous gas diffusion and catalyst layers, the magnitude of the effective electronic conductivity is determined in terms of the porosity in accordance with the Bruggemann's equation as

$$\sigma_{\text{GDL}}^{\text{eff}} = (1 - \varepsilon_{\text{GDL}})^{\chi_{\text{GDL}}} \sigma_{\text{GDL}} \tag{8a}$$

$$\sigma_{\text{Cat}}^{\text{eff}} = \varepsilon_{\text{S,Cat}}^{\chi_{\text{Cat}}} \sigma_{\text{S,Cat}} \tag{8a}$$

It is noticed that the effective electronic conductivity of the catalyst layer ($\sigma_{\text{Cat}}^{\text{eff}}$) increases with the volume fraction of solid catalyst particles in catalyst layer ($\varepsilon_{\text{S,Cat}}$). In addition, the source term ζ in Eq. (7) is zero for the carbon plates or the GDL without electrochemical reaction. When the catalyst layers is dealt with, ζ is equal to the transfer current densities $-j_{\text{a}}$ and j_{c} for the anode and the cathode, respectively, which are calculated with Eqs. (6a) and (6b).

2.1.4. Ionic conduction (catalyst layers and proton exchange membrane)

The protons of hydrogen (H^+) are generated in the anode catalyst layer and then migrate through the proton exchange membrane toward the cathode catalyst layer to react with oxygen and the returning electrons. Therefore, ionic conduction occurs in the catalyst layers and the proton exchange membrane.

The ionic conduction equation for determination of the phase potential (φ) in the catalyst layers is

$$-\nabla \cdot (\Gamma_{\text{Cat}}^{\text{eff}} \nabla \varphi_{\text{Cat}}) = \zeta \tag{9}$$

where φ_{Cat} is the phase potential and $\Gamma_{\text{Cat}}^{\text{eff}}$ is the effective ionic conductivity of the catalyst layers. Note that the source term ζ is identical to that of Eq. (7). The effective ionic conductivity $\Gamma_{\text{Cat}}^{\text{eff}}$ is evaluated by using

$$\Gamma_{\text{Cat}}^{\text{eff}} = \varepsilon_{\text{N,Cat}}^{\chi_{\text{Cat}}} \Gamma_{\text{N,Cat}} \tag{10}$$

It is important to note that since the content of Nafion in the catalyst layers help reduce the ionic resistance, the effective ionic conductivity of the catalyst layer ($\Gamma_{\text{Cat}}^{\text{eff}}$) increases with the volume fraction of Nafion in catalyst layer ($\varepsilon_{\text{N,Cat}}$).

On the other hand, the ionic conduction equation for the membrane is expressed as

$$\nabla \cdot (\Gamma_m \nabla \varphi_m) = 0 \tag{11}$$

where φ_m is the phase potential and Γ_m is the ionic conductivity of the membrane. The expression for ionic conductivity of the membrane has been proposed by Springer et al. [16] as:

$$\Gamma_m(T) = \exp\left[1268\left(\frac{1}{303} - \frac{1}{T}\right)\right](0.005239\lambda - 0.00326) \tag{12}$$

where the water content of the membrane (λ) is dependent on the dimensionless water activity in the membrane (a) according to experimental data. The activity is assumed uniform over the membrane, which is defined as the gas partial pressure of water at equilibrium with the membrane divided by the saturation pressure of water vapor at the operating temperature. That is

$$a = \frac{X_{H_2O} P}{P_{sat}} \tag{13}$$

where the saturation pressure of water vapor can be computed from

$$\begin{aligned}\log_{10} P_{sat} = {} & -2.1794 + 0.02953(T - 273.15) - 9.1837 \\ & \times 10^{-5}(T - 273.15)^2 + 1.4454 \\ & \times 10^{-7}(T - 273.15)^3\end{aligned} \tag{14}$$

with T in K. The correlation between λ and a is derived as

$$\lambda = \begin{cases} 0.043 + 17.81a - 39.85a^2 + 36a^3 & 0 \le a \le 1 \\ 14 + 1.4(a-1) & 1 < a \le 3 \end{cases} \tag{15}$$

Based on the solutions for the phase potential (φ), the distribution of local ionic current density (i_i) may be further determined with $\vec{i} = -\Gamma \nabla \varphi$.

2.1.5. Nafion loading (catalyst)

As mentioned earlier, Nafion is an electronic insulator. Hence, when it is introduced into the catalyst layer, it decreases the electronic conductivity of the catalyst layer. However, on the other hand, since it is a good conductor for the hydrogen protons, Nafion loading can elevate the ionic conductivity of the catalyst layers. Besides, the introduction of Nafion into the catalyst layers changes simultaneously the porosity and the gas permeability of the layers so that it affects the transport of the gas species. As Nafion is loaded, total volume of the catalyst layer (υ_t) may be divided into three major portions, namely, the volume occupied by the solid catalyst particles (υ_S), the volume occupied by Nafion (υ_N), and the volume of the void space (υ_V). The volume fractions of the three portions are denoted by $\varepsilon_{S,Cat}$, $\varepsilon_{N,Cat}$, and $\varepsilon_{V,Cat}$, respectively, and are defined as

$$\varepsilon_{S,Cat} = \frac{\upsilon_S}{\upsilon_t} \tag{16a}$$

$$\varepsilon_{N,Cat} = \frac{\upsilon_N}{\upsilon_t} \tag{16b}$$

and

$$\varepsilon_{V,Cat} = 1 - \varepsilon_{C,Cat} - \varepsilon_{N,Cat} \tag{16c}$$

It is noted that the present model does not include the effects of heat and liquid water accumulation. A more powerful model will absolutely be desired when necessary.

2.1.6. Solution domain and boundary conditions

For the pattern of straight parallel channels shown in Fig. 1, as the number of gas channels is large enough, a periodic transport phenomenon is expected to develop from channel to channel. Thus, one only needs to deal with the solution domain of a single module indicated by the dashed lines. In this study, the width of a module (l_P) is set to be 1 mm. Therefore, for the faces of solution domain at $x = 0$ and 1 mm, a symmetric boundary condition for $\vec{U}$, Y, ϕ, and φ is prescribed.

Solid walls of the gas channels or the carbon plates are impermeable, and hence, on the solid walls, $\partial Y_i/\partial n = 0$ and $\vec{U} = 0$. In addition, since both the gas channels and the membrane are insulators against electrons; at the boundaries of these two components, the normal gradient of the electric potential (ϕ) is vanished. Furthermore, the ionic conduction takes place only inside the catalyst layer and proton exchange membrane, and the protons are not allowed to transfer into other components; therefore, on the faces of the catalyst layer and the membrane the normal gradient of phase potential is assigned to be zero.

As to the inlet conditions, the inlet velocities for the anode gas (hydrogen) and the cathode gas (air) in the gas channel, V_a and V_c, are fixed at 0.3 and 0.5 m s^{-1}, respectively. The inlet mass fractions for all the gas species are specified, and their values are provided in Table 1. Note that both the fuel and the oxidant gases enter the fuel cell at 100% relative humidity. On the other hand, for the boundary conditions at the exit, it is assumed that the flow becomes fully developed downstream. Thus, the exit boundary conditions may be described as

$$u = w = \frac{\partial v}{\partial y} = \frac{\partial Y_i}{\partial y} = \frac{\partial \phi}{\partial y} = \frac{\partial \varphi}{\partial y} = 0 \tag{17}$$

2.2. Numerical methods

These above set of conservation equations along with the property equations are solved by adopting a finite-volume scheme on structured grids within the framework of the commercial computational fluid dynamics code (CFD-ACE+). A self-developed subroutine has been built for calculating the values of the properties of the catalyst layers, including the effective electronic conductivity, the effective ionic conductivity, and effective mass diffusivity of gas species (σ_{Cat}^{eff}, Γ_{Cat}^{eff}, and D_i^{eff}) for various Nafion loading conditions. The Nafion loading condition is specified by adjusting relatively the values of volume fractions of Nafion loaded, solid catalyst particles, and void space inside the catalyst layers ($\varepsilon_{N,Cat}$, $\varepsilon_{S,Cat}$, and $\varepsilon_{V,Cat}$). The self-developed subroutine is incorporated with the computational fluid dynamics code through a Python-interface connection. The message of any change in the Nafion content is firstly used by the self-developed subroutine to update the values of the properties of

Table 3
Specification of single cell module and test conditions in experiments

Cross-sectional area	22 cm × 22 cm
Active area of membrane	14 cm × 14 cm
Membrane	Five-layer (Dupont)
Carbon plates	Composite graphite plate (3-mm thickness)
Inlet conditions of hydrogen	$T = 80\,^{\circ}C$ and RH = 100%
Inlet conditions of air	$T = 80\,^{\circ}C$ and RH = 100%
Volumetric flow rate of hydrogen	1500 sccm
Volumetric flow rate of air	2500 sccm

the catalyst layer, and then the updated values of the catalyst layer properties can be transmitted automatically to the computational fluid dynamics code through the interface in order for solution of the three-dimensional transport phenomena taking place in the PEMFC. When necessary, the CFD code solutions may also be sent back to the self-developed subroutine through the interface for further computation.

In an average case, the structured grids containing approximately 100,000 to 200,000 control volumes are used. A grid-independence check has been performed to ensure the accuracy of the numerical solutions. At each iteration step, the iteration for the solutions for $\vec{U}$, Y, ϕ, and φ is progressed until the following convergence criterion is satisfied:

$$\left|\frac{(\Psi^{l}_{i,j,k} - \Psi^{l-1}_{i,j,k})}{\Psi^{l-1}_{i,j,k}}\right| \leq 10^{-6} \tag{18}$$

where Ψ represents each of the variables $\vec{U}$, Y, ϕ, and φ; l the iteration number; and i, j, and k represent the spatial indices for the x-, y-, and z-directions, respectively.

The average current density (**I**) of fuel cells is calculated by integration of local electric current density distribution on the carbon plate surface at $z = 0$ divided by the carbon plate surface area as

$$\mathbf{I} = \frac{1}{A}\int_{0}^{A} i_s \cdot \mathrm{d}A \tag{19}$$

where i_s is the local electric current density on the carbon plate surface and A is the carbon plate surface area. In the mean time, the gas channel width fraction (Λ) is defined by the ratio of the gas channel width (l_C) to the width of a module (l_P), that is

$$\Lambda = \frac{l_C}{l_P} \tag{20}$$

3. Experiments with single-cell PEMFC

A single-cell fuel cell module with cross-sectional area of 22 cm × 22 cm and active area of 14 cm × 14 cm has been installed and tested to partly verify the numerical predictions yielded by the commercial computational fluid dynamics code. The specification of the single cell module and the test conditions are given in Table 3. The purpose of the experiments is simply to test the validity of the CFD code; therefore, Nafion is not yet introduced into the catalyst layers of the MEA. The operating and geometrical conditions in simulation are consistent with the

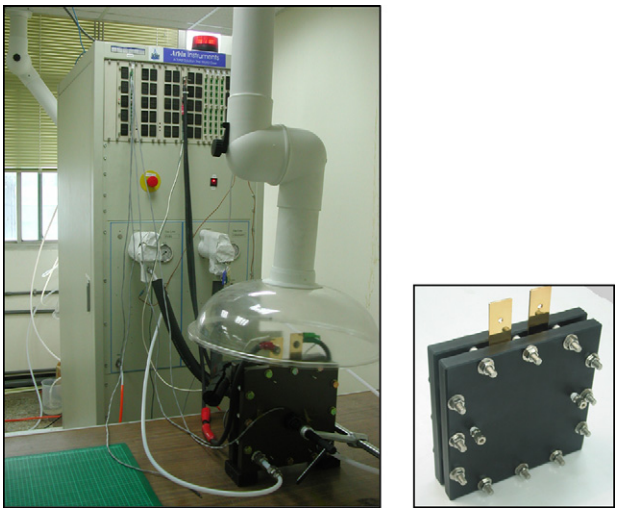

Fig. 2. Experimental apparatus (left) and single-cell fuel cell module (right).

experimental module. Two composite graphite plates of 3-mm thickness are used as the flow fields and current conductors. A five-layer membrane exchange assembly (MEA) provided by Dupont Inc. is placed at the center between the two composite graphite plates. The membrane used in this MEA is Nafion® 112 and the gas diffusion layers are made of carbon fiber paper. Before entering the channels, the fuel and oxidant gases are humidified to maintain at 100% relative humidity and 80 °C temperature.

In addition, to obtain the polarization curves with the fuel cell, a performance test system has also been setup. In the experiments, the volumetric flow rates of the hydrogen and the air are typically maintained at 1500 and 2500 sccm, corresponding to $V_a = 0.3\ \mathrm{m\,s^{-1}}$ and $V_c = 0.5\ \mathrm{m\,s^{-1}}$, respectively. The fuel cell temperature is maintained at 343 K. Photographs of the experimental apparatus and the single-cell fuel cell module are shown in Fig. 2.

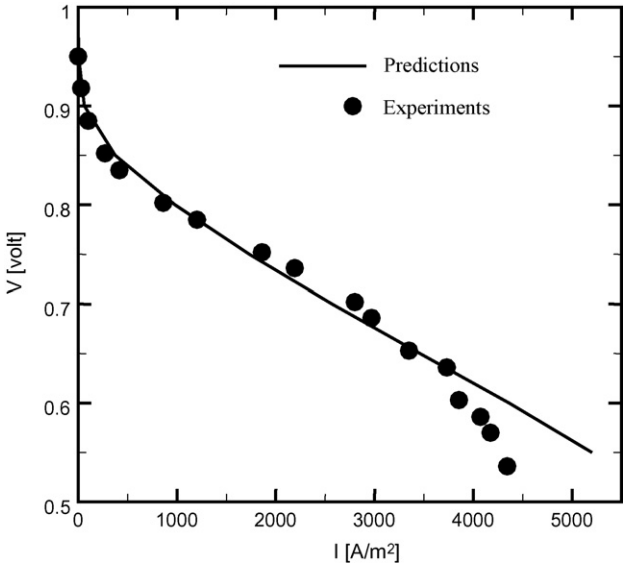

Fig. 3. Polarization curves: comparison between predictions and experiments.

Fig. 3 shows a comparison between the numerical predictions and the experiment data for the polarization curves of the single-cell fuel cell module without Nafion loading. The operating conditions have been described in the preceding section. It is observed that the numerical predictions closely agree with the experiments, especially as $\mathbf{I} < 3800\,\mathrm{A\,m^{-2}}$. The difference between the two sets of data becomes appreciable only in the high-current-density regime. In this regime, the experimental data appear to experience a greater drop in the operating voltage than the predicted. The greater voltage drop is attributed to the concentration loss due to insufficient supply of O_2 and H_2 in experiments at the cathode and the anode, respectively which is remarkable in the high current density situations. In Fig. 3, it is found that at $\mathbf{V} = 0.7$ V the numerical and the experimental data for the current density are in close agreement (at approximately $2500\,\mathrm{A\,m^{-2}}$). Thus, the typical value of the operating voltage of the fuel cell is fixed at 0.7 V in the present study to evaluate the Nafion loading effects. Note that in the following parametric study, the operating temperature is assigned to be 323 K. However, the experiments have been performed at different temperatures. The purpose of the experiments is simply to test the validity of the CFD code; therefore, only the data at 343 K are shown in Fig. 3.

4. Results and discussion

Parametric study of the effects of the parameters listed in Tables 1 and 2 is now carried out to evaluate the performance of PEMFC under various combinations of these parameters.

Nafion loading effects on the distributions of mass fractions of hydrogen and oxygen at the anode and the cathode, respectively, are shown in Fig. 4. Numerical solutions on

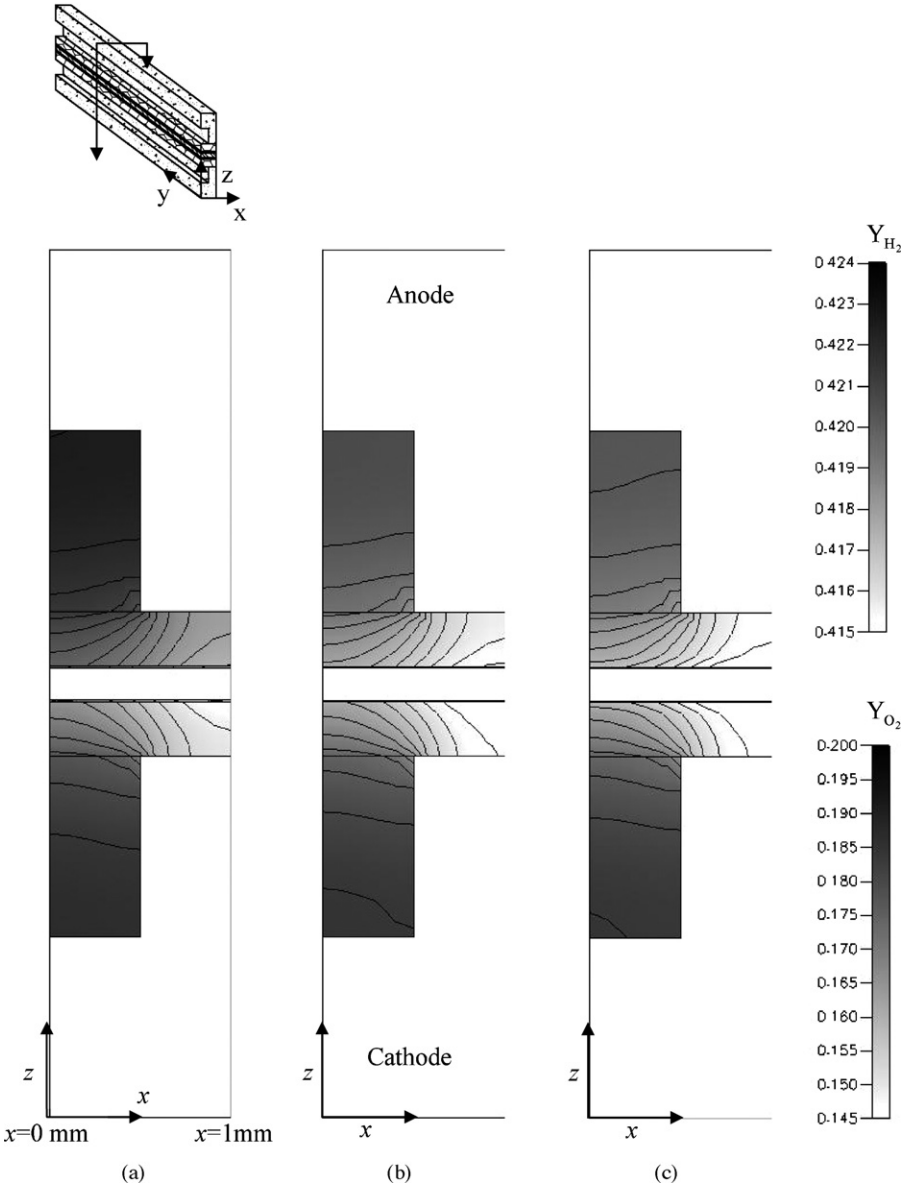

Fig. 4. Mass fraction distributions on cross-section at $y = 25$ mm with different volume fractions of Nafion in catalyst layer, for $\mathbf{V} = 0.7$ V, $\varepsilon_{GDL} = 0.5$, $\varepsilon_{S,Cat} = 0.885$, $l_C = 5 \times 10^{-4}$ m, $t_{GDL} = 3 \times 10^{-4}$ m, $t_m = 1.76 \times 10^{-4}$ m, $h = 1 \times 10^{-3}$ m, and $\Lambda = 0.5$. (a) $\varepsilon_{N,Cat} = 0.1$; (b) $\varepsilon_{N,Cat} = 0.2$; (c) $\varepsilon_{N,Cat} = 0.3$.

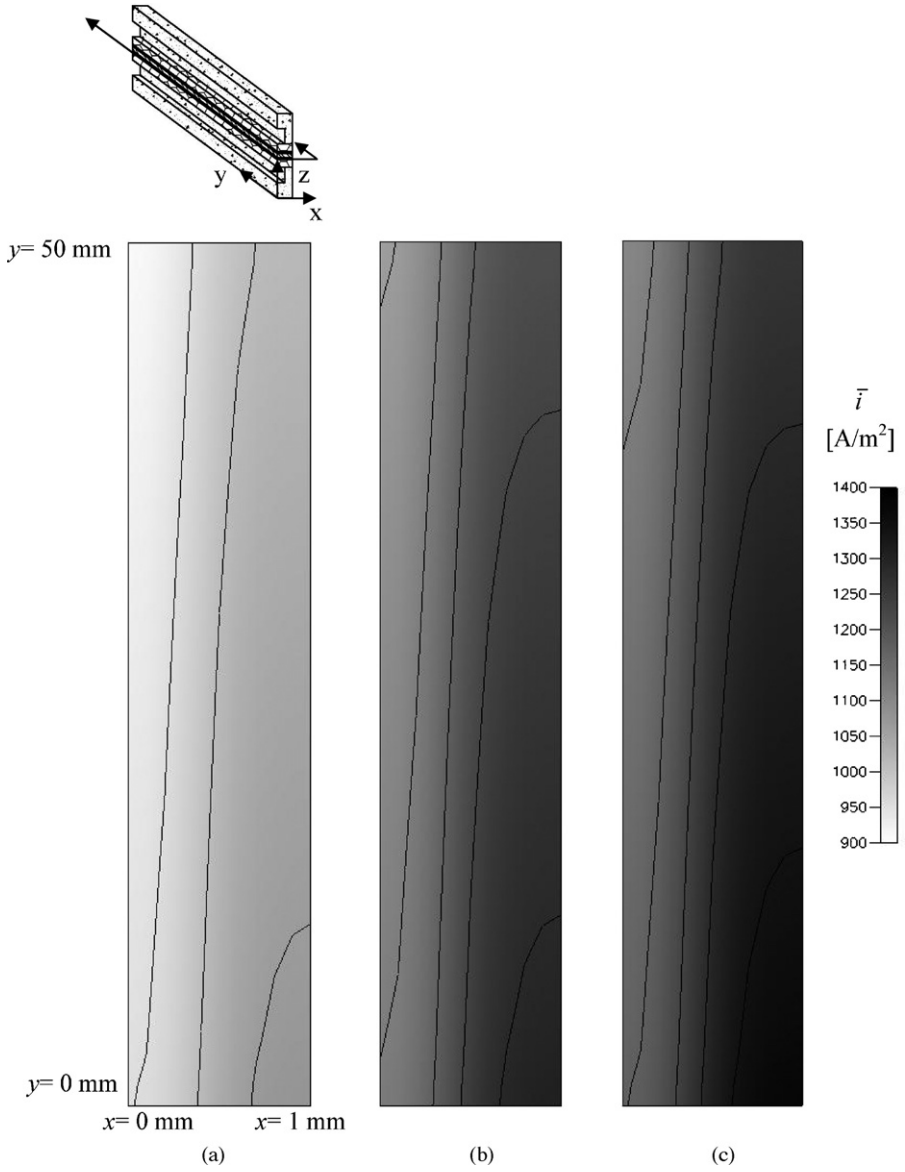

Fig. 5. Planar distribution of ionic current density at the center plane of the cathode catalyst layer with different volume fractions of Nafion in catalyst layer, for $\mathbf{V} = 0.7$ V, $\varepsilon_{GDL} = 0.5$, $\varepsilon_{S,Cat} = 0.885$, $l_C = 5 \times 10^{-4}$ m, $t_{GDL} = 3 \times 10^{-4}$ m, $t_m = 1.76 \times 10^{-4}$ m, $h = 1 \times 10^{-3}$ m, and $\Lambda = 0.5$. (a) $\varepsilon_{N,Cat} = 0.1$; (b) $\varepsilon_{N,Cat} = 0.2$; (c) $\varepsilon_{N,Cat} = 0.3$.

cross section at $y = 25$ mm with different volume fractions of Nafion in catalyst layer ($\varepsilon_{N,Cat} = 0.1$, 0.2, and 0.3) are plotted, for $\mathbf{V} = 0.7$ V, $\varepsilon_{GDL} = 0.5$, $\varepsilon_{S,Cat} = 0.885$, $t_{GDL} = 5 \times 10^{-4}$ m, $t_m = 1.76 \times 10^{-4}$ m, $h = 1 \times 10^{-3}$ m, and $\Lambda = 0.5$. It is expected that the introduction of Nafion reduces the porosity of the catalyst layers; therefore, the mass fractions of the reactant gases in the catalyst layers are obviously decreased by elevating the volume fraction of Nafion. However, since Nafion loading can elevate the ionic conductivity of the catalyst layers, the current density may be increased by the introduction of Nafion. For example, Fig. 5 displays the planar distribution of the ionic current density at the center plane of the cathode catalyst layer in the same conditions of Fig. 4. It is clearly seen that the uniformity of the ionic current density distribution on the plane is significantly improved by increasing the volume fraction of Nafion in catalyst layer. In accordance with the discussion concerning the gases transport and the ionic conduction discussed herein, an optimal Nafion content in the catalyst layer is indeed expected and desired.

Given the operating conditions of $\mathbf{V} = 0.7$ V, $\varepsilon_{GDL} = 0.5$, $\varepsilon_{S,Cat} = 0.588$, $t_{GDL} = 5 \times 10^{-4}$ m, $t_m = 1.76 \times 10^{-4}$ m, $h = 1 \times 10^{-3}$ m, and $\Lambda = 0.5$, one may examine the dependence of power density of the PEMFC (**P**) on the volume fraction of Nafion in the catalyst layer ($\varepsilon_{N,Cat}$). The predicted results are plotted in Fig. 6. It is clearly seen that the magnitude of the power density first increases with $\varepsilon_{N,Cat}$ to reach its optimal value of approximately 1812 W m^{-2} at $\varepsilon_{N,Cat} = 0.3$, and then it descends when the value of $\varepsilon_{N,Cat}$ over the optimal one.

The data shown in Fig. 6 are collected as the volume fraction of solid catalyst particles in the catalyst layer ($\varepsilon_{S,Cat}$) is fixed at 0.588. On the other hand, what plotted in Fig. 7 is the information concerning the dependence of power density on $\varepsilon_{N,Cat}$

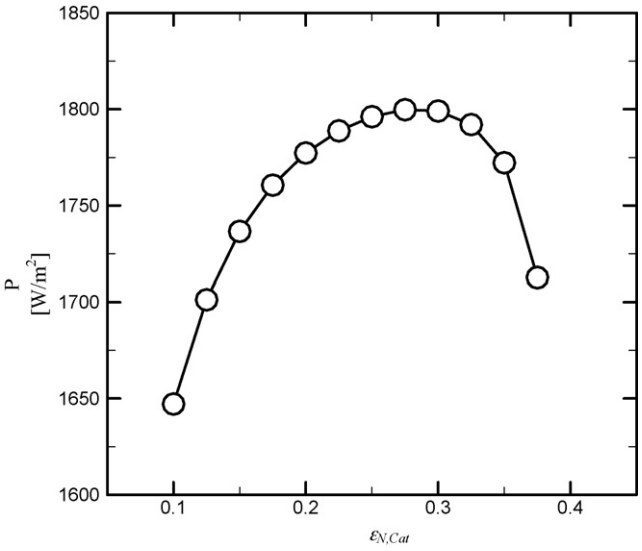

Fig. 6. Power density as a function of volume fraction of Nafion in catalyst layer at $\mathbf{V} = 0.7$ V, $\varepsilon_{GDL} = 0.5$, $\varepsilon_{S,Cat} = 0.588$, $l_C = 5 \times 10^{-4}$ m, $t_{GDL} = 3 \times 10^{-4}$ m, $t_m = 1.76 \times 10^{-4}$ m, $h = 1 \times 10^{-3}$ m, and $\Lambda = 0.5$.

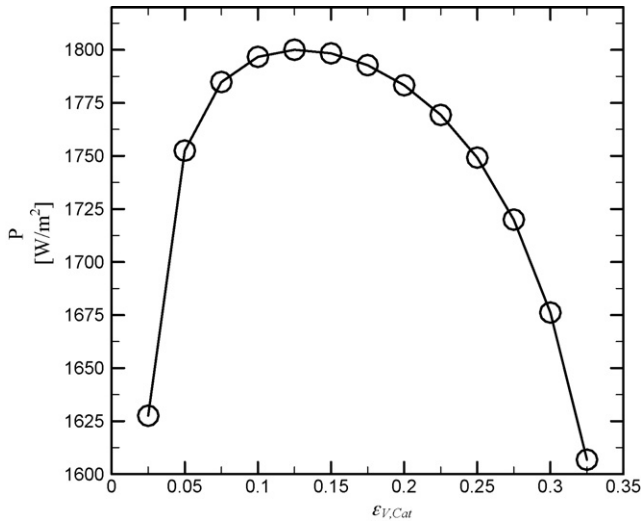

Fig. 8. Power density as a function of volume fraction of void space in catalyst layer at $\mathbf{V} = 0.7$ V, $\varepsilon_{GDL} = 0.5$, $\varepsilon_{S,Cat} = 0.588$, $l_C = 5 \times 10^{-4}$ m, $t_{GDL} = 3 \times 10^{-4}$ m, $t_m = 1.76 \times 10^{-4}$ m, $h = 1 \times 10^{-3}$ m, and $\Lambda = 0.5$.

at a constant volume fraction of void space in the catalyst layer ($\varepsilon_{V,Cat}$). Note that the solid volume fraction is reduced as more Nafion is added while the void space stays constant. Again, the curve exhibits a peak value as $\varepsilon_{N,Cat}$ is varied from 0.1 to 0.8. Results proved in Fig. 7 illustrates that in this case the maximum power density can be yielded when the volume fraction of Nafion in the catalyst layer is maintained at 0.45.

Fig. 8 shows the variation of power density with the volume fraction of void space in the catalyst layer for $\mathbf{V} = 0.7$ V, $\varepsilon_{GDL} = 0.5$, $\varepsilon_{N,Cat} = 0.3$, $l_C = 5 \times 10^{-4}$ m, $t_{GDL} = 3 \times 10^{-4}$ m, $t_m = 1.76 \times 10^{-4}$ m, $h = 1 \times 10^{-3}$ m, and $\Lambda = 0.5$. The volume fraction of void space in the catalyst layer ($\varepsilon_{V,Cat}$) is also referred to as the porosity of the catalyst layer. For this case, the ionomer content stays constant and in order to increase porosity only the solid phase is decreased. An increase in $\varepsilon_{V,Cat}$ is favorable for sufficient gas supply; however, it reduces the electronic conduction. For the case considered in this figure, it is observed that the optimal power density is reached at $\varepsilon_{V,Cat} = 0.125$.

Fig. 9 further conveys the effects of gas channel width fraction (Λ) on the performance of the fuel cell at $\mathbf{V} = 0.7$ V, $\varepsilon_{GDL} = 0.5$, $\varepsilon_{V,Cat} = 0.112$, $\varepsilon_{N,Cat} = 0.3$, $t_{GDL} = 3 \times 10^{-4}$ m, $t_m = 1.76 \times 10^{-4}$ m, and $h = 1 \times 10^{-3}$ m. It is observed that indeed the channel width fraction has subtle influence on the cell performance. Larger channel width fraction means a larger area occupied by the gas channels and more reactant gases are supplied; however, it also means thinner ribs and hence smaller area for electron conduction. Therefore, the ohmic impedance increases with the channel width fraction. With these two opposing effects, there must exists an optimal value of the gas channel

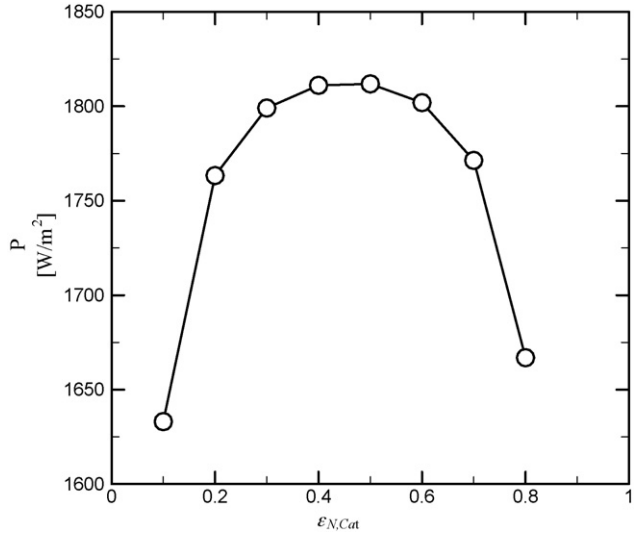

Fig. 7. Power density as a function of volume fraction of Nafion in catalyst layer at $\mathbf{V} = 0.7$ V, $\varepsilon_{GDL} = 0.5$, $\varepsilon_{V,Cat} = 0.112$, $l_C = 5 \times 10^{-4}$ m, $t_{GDL} = 3 \times 10^{-4}$ m, $t_m = 1.76 \times 10^{-4}$ m, $h = 1 \times 10^{-3}$ m, and $\Lambda = 0.5$.

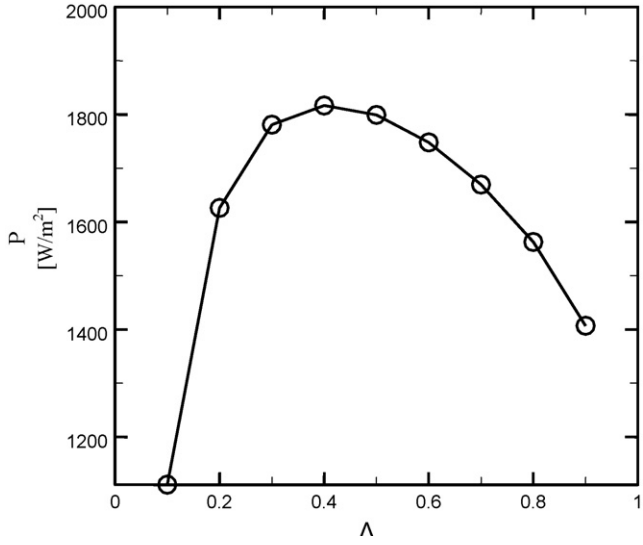

Fig. 9. Power density as a function of channel width fraction at $\mathbf{V} = 0.7$ V, $\varepsilon_{GDL} = 0.5$, $\varepsilon_{V,Cat} = 0.112$, $\varepsilon_{N,Cat} = 0.3$, $t_{GDL} = 3 \times 10^{-4}$ m, $t_m = 1.76 \times 10^{-4}$ m, and $h = 1 \times 10^{-3}$ m.

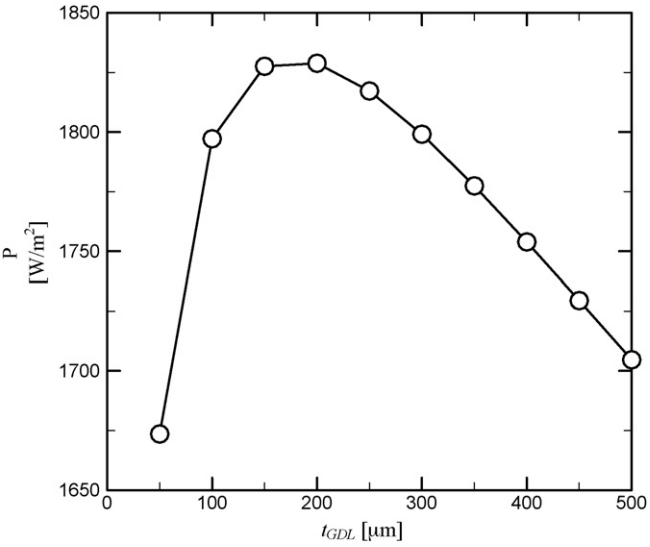

Fig. 10. Power density as a function of thickness of gas diffusion layer at $\mathbf{V} = 0.7$ V, $\varepsilon_{GDL} = 0.5$, $\varepsilon_{V,Cat} = 0.112$, $\varepsilon_{N,Cat} = 0.3$, $l_C = 5 \times 10^{-4}$ m, $t_m = 1.76 \times 10^{-4}$ m, $h = 1 \times 10^{-3}$ m, and $\Lambda = 0.5$.

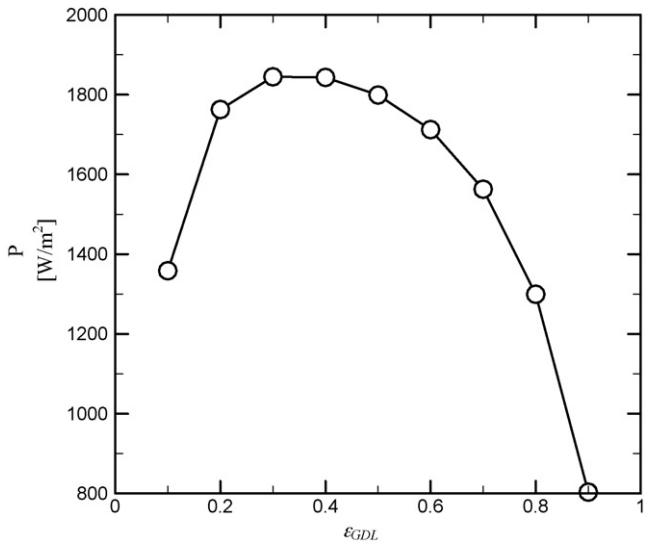

Fig. 11. Power density as a function of porosity of gas diffusion layer at $\mathbf{V} = 0.7$ V, $\varepsilon_{V,Cat} = 0.112$, $\varepsilon_{N,Cat} = 0.3$, $l_C = 5 \times 10^{-4}$ m, $t_{GDL} = 3 \times 10^{-4}$ m, $t_m = 1.76 \times 10^{-4}$ m, $h = 1 \times 10^{-3}$ m, and $\Lambda = 0.5$.

width fraction. In Fig. 9, the results show that the largest power of 1816 W m^{-2} is obtained at the optimal gas channel width fraction of $\Lambda = 0.4$ under the conditions considered in this case.

Plotted in Fig. 10 is the variation in the power density with the thickness of gas diffusion layer (t_{GDL}) for $\mathbf{V} = 0.7$ V, $\varepsilon_{GDL} = 0.5$, $\varepsilon_{V,Cat} = 0.112$, $\varepsilon_{N,Cat} = 0.3$, $l_C = 5 \times 10^{-4}$ m, $t_m = 1.76 \times 10^{-4}$ m, $h = 1 \times 10^{-3}$ m, and $\Lambda = 0.5$. A thicker gas diffusion layer may allow the gas to disperse uniformly in the entire gas diffusion layer; however, it also tends to increase the electric resistance against the conduction of electrons. It is seen that the optimal performance of the fuel cell is 1828 W m^{-2} at $t_{GDL} = 200$ μm. In addition, the porosity of the gas diffusion layer (ε_{GDL}) is also one of the major factors affecting the fuel cell performance. Similarly, an increase in ε_{GDL} is favorable for sufficient gas supply; however, it also tends to increase the electric resistance. For the case at $\mathbf{V} = 0.7$ V, $\varepsilon_{V,Cat} = 0.112$, $\varepsilon_{N,Cat} = 0.3$, $l_C = 5 \times 10^{-4}$ m, $t_{GDL} = 3 \times 10^{-4}$ m, $t_m = 1.76 \times 10^{-4}$ m, $h = 1 \times 10^{-3}$ m, and $\Lambda = 0.5$, the results shown in Fig. 11 illustrate that the peak value of the power density can be achieved at $\varepsilon_{GDL} = 0.3$.

Attention is now drawn to the effects of the thickness of the proton exchange membrane on the performance of fuel cell. Fig. 12 displays the dependence of power density on the thickness of the membrane (t_m) at $\mathbf{V} = 0.7$ V, $\varepsilon_{GDL} = 0.5$, $\varepsilon_{V,Cat} = 0.112$, $\varepsilon_{N,Cat} = 0.3$, $l_C = 5 \times 10^{-4}$ m, $t_{GDL} = 3 \times 10^{-4}$ m, $h = 1 \times 10^{-3}$ m, and $\Lambda = 0.5$. It is noticed that within the range between $t_m = 50$ and 500 μm, the power density of the fuel cell is monotonically decreased by increasing the thickness of the membrane, and hence, no optimal membrane thickness is observed. This reflects the fact that a thicker membrane possessing higher mechanical strength is also a membrane possessing higher ionic resistance. However, the other important aspect of the membrane thickness effects is that the cross-over current, which reduces the performance of a fuel cell, increases with decreasing membrane thickness. Therefore, it is not true that thinner membranes are always better.

It is important to mention that in order to be able to report optimal conditions for more than one design variable, a multivariable numerical optimization problem (e.g. Lin et al. [10], Song et al. [13,14], and Secanell et al. [15]) is necessary. A good example of the need for such an approach is the difference in optimum Nafion content between Figs. 6 and 7 for which a single parameter was changed. Further, the optimum channel width fraction is 0.4 only for a GDL with 0.5 porosity and a catalyst layer with 0.112 porosity and 0.3 volume fraction of ionomer. This value might be completely different for a catalyst layer with 0.8 porosity.

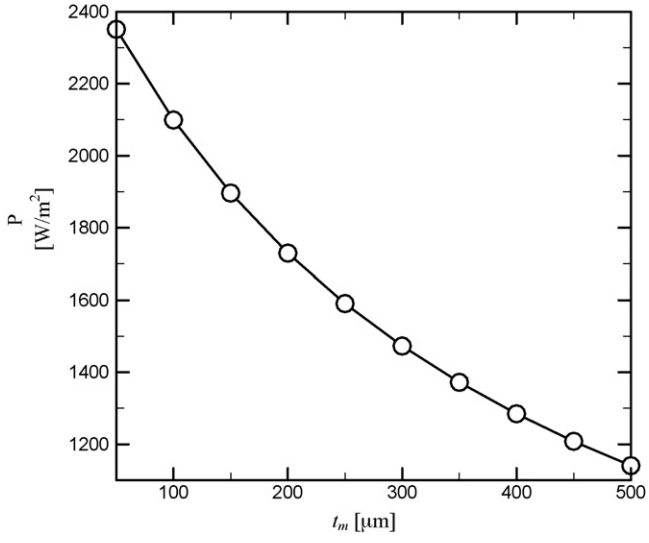

Fig. 12. Power density as a function of thickness of the membrane at $\mathbf{V} = 0.7$ V, $\varepsilon_{GDL} = 0.5$, $\varepsilon_{V,Cat} = 0.112$, $\varepsilon_{N,Cat} = 0.3$, $l_C = 5 \times 10^{-4}$ m, $t_{GDL} = 3 \times 10^{-4}$ m, $h = 1 \times 10^{-3}$ m, and $\Lambda = 0.5$.

5. Conclusions

This study is concerned with the Nafion loading effects by numerical simulation using a full-cell three-dimensional numerical model. In addition, change in the performance of the PEMFC accompanying various combinations of geometric parameters is also investigated. A 22 cm × 22 cm single-cell fuel cell module with 14 cm × 14 cm active area has been installed and tested. Part of the numerical results is compared with experiments for validation. It has been observed that the numerical predictions closely agree with the experiments, especially as $\mathbf{I} < 3800\ \mathrm{A\,m^{-2}}$.

A self-developed subroutine has been built for calculating the values of the properties of the catalyst layers, including the effective electronic conductivity, the effective ionic conductivity, and effective mass diffusivity of gas species for various Nafion loading conditions. The self-developed subroutine is incorporated with a computational fluid dynamics code through a Python-interface connection to deal with the three-dimensional mass, momentum, and species transport phenomena as well as the electron- and proton-transfer process taking place in the PEMFC.

For the particular cases considered in this study, the optimal conditions of the volume fraction of Nafion in the catalyst layer ($\varepsilon_{N,Cat}$), the volume fraction of void space in the catalyst layer ($\varepsilon_{V,Cat}$), the gas channel width (l_C), and the thickness and porosity of the gas diffusion layer (t_{GDL} and ε_{GDL}), which lead to a higher fuel cell power density, are investigated. Power density of the fuel cell is monotonically decreased by increasing the thickness of the membrane (t_m), and hence, no optimal membrane thickness is observed. Note that the suggested optimal parameters are obtained under the base case conditions considered in the present study. When the conditions are changed, the optimal values of these parameters may be altered. Therefore, in order to be able to report optimal conditions for more than one design variable, a multivariable numerical optimization problem is necessary.

Acknowledgements

The authors would like to thank the National Science Council, Taiwan, ROC, for their financial support under Grant: NSC 93-2212-E-036-001. Authors would also like to thank Tatung Company for their support of the performance test system.

References

[1] C.C. Boyer, R.G. Anthony, A.J. Appleby, J. Appl. Electrochem. 30 (2000) 777–786.
[2] E. Passalacqua, F. Lufrano, G. Squadrito, A. Patti, L. Giorgi, Electrochim. Acta 43 (1998) 3665–3673.
[3] E. Passalacqua, F. Lufrano, G. Squadrito, A. Patti, L. Giorgi, Electrochim. Acta 46 (2001) 799–805.
[4] E. Antolini, L. Giorgi, A. Pozio, E. Passalacqua, J. Power Sources 77 (1999) 136–142.
[5] Z. Qi, A. Kaufman, J. Power Sources 113 (2003) 37.
[6] F. Lufrano, P. Staiti, M. Minutoli, J. Electrochem. Soc. 151 (2004) A64–A68.
[7] J.T. Wang, R.F. Savinell, Electrochim. Acta 37 (1992) 2737–2745.
[8] J.S. Yi, T.V. Nguyen, J. Electrochem. Soc. 146 (1999) 38–45.
[9] V. Gurau, F. Barbir, H. Liu, J. Electrochem. Soc. 147 (2000) 4485–4493.
[10] H.H. Lin, C.H. Cheng, C.Y. Soong, F. Chen, W.M. Yan, J. Power Sources 162 (2006) 246–254.
[11] E. Hontanon, M.J. Escudero, C. Bautista, P.L. Garcia-Ybarra, L. Daza, J. Power Sources 86 (2000) 363–368.
[12] T. Berning, N. Djilali, J. Power Sources 124 (2003) 440–452.
[13] D. Song, Q. Wang, Z. Liu, T. Navessin, M. Eikerling, S. Holdcroft, J. Power Sources 126 (2004) 104.
[14] D. Song, Q. Wang, Z. Liu, T. Navessin, M. Eikerling, Z. Xie, T. Navessin, S. Holdcroft, Electrochim. Acta 50 (2005) 3347–3358.
[15] M. Secanell, B. Carnes, A. Suleman, N. Djilali, Electrochim. Acta, in press, doi:10.1016/j.electacta.2006.09.049.
[16] T.E. Springer, T.A. Zawodzinski, S. Gottesfeld, J. Electrochem. Soc. 138 (1991) 2334–2342.